JTTEE5 12:44-52

Peer Reviewed

Control of Thermal Spray Processes by Means of Process Maps and Process Windows

Martin Friis and Christer Persson

(Submitted 18 September 2001; in revised form 20 December 2001)

A general method to map and control thermal spray processes, ensuring predefined levels of selected final coating properties, is presented. The method relies on monitoring and individually controlling particle velocity and particle temperature through selected spray gun parameters. Mapping of the process results in process maps describing the individual effect of particle velocity and particle temperature on each selected coating property of concern; in this case, different features of the microstructure and deposition efficiency. From the information provided by the process maps, a process window is constructed. This process window provides the limits within which particle velocity and particle temperature are allowed to vary to fulfill a predefined coating specification. To verify the method, two predefined thermal barrier top coatings—one porous and one dense—were produced by air plasma spray with satisfactory results.

Keywords dpv 2000, microstructure, particle temperature, particle velocity, plasma spray, process control, process map, process window

1. Introduction

The thermal and mechanical properties and the life of a plasma sprayed ceramic coating depend on the coating microstructure. Therefore, the ability to create a desired microstructure is of vital importance to produce a coating that is optimized for its applications.

Generally, the plasma spray process is controlled by an iterative procedure, namely, setting the process parameters, spraying, and evaluating the samples. This procedure is repeated until certain standards are obtained, and then the parameter setting is padlocked. A more efficient approach is to perform and evaluate factorial designed experiments from which the relationship between the spray gun parameters and the coating properties can be found and used to optimize and control the process.

Drawbacks of these approaches are the low reproducibility and quality standards achieved, together with the long lead-time between production of the coating and the destructive sample evaluation, resulting in a very time-consuming and expensive manufacturing process.

Thermal spray processes are influenced by parameters of two different types. The spray gun parameters affect the plasma plume, and thereby, the particles. Other parameters do not affect the plume, but instead, have a direct influence on the coating build-up. The parameters having a direct effect on the coating are usually set to constant values. Due to the large velocity and temperature gradients in the plume, small variations in uncontrollable spray gun parameters such as the nozzle geometry, powder inlet geometry, and wear of the cathode, as well as fluctuations in the controllable spray gun parameters, might result in significant changes in the particle properties.

Therefore, control of the process by monitoring and controlling the particle properties seems a promising approach in two aspects. By moving the control of the process from the spray gun parameters to the particle properties, the uncertainties deriving from controllable as well as uncontrollable parameters will be eliminated. Moreover, it then suffices for a few particle properties to be attended to, instead of the numerous spray gun parameters.

Our objective here is to present how the process can be controlled through monitoring and controlling the particle properties. This is achieved through construction of reliable process maps, i.e., maps describing each specific coating property as a function of particle properties. The process maps, in turn, are used to construct a process window providing the limits within which the particle properties are allowed to vary for the desired coating to be produced. The method presented is general and should be applicable to any thermal spray process. In this work, however, experimental verification has been performed on a thermal barrier top coating, air plasma sprayed, with a zirconia powder.

2. Process Maps and Process Windows

A process map is the visualization of a mathematical model describing the influence of particle properties on one critical coating property. Such a coating property can be, for instance, the coating microstructure, any mechanical or thermal property, e.g., hardness, thermal conductivity, or even an economical aspect such as the deposition efficiency. Each such map is restricted to one specific spray gun, one specific powder, and with all other parameters, except the ones used to control the particle properties, set at constant values. For other spray guns and powders the appearance of the process maps will be different, although the concept is the same.

A prerequisite for creation of process maps is to define and, with a sufficient degree of accuracy, be able to measure relevant

Martin Friis, University Trollhattan/Uddevalla, S-461 29 Trollhattan, Sweden; and **Christer Persson**, Division of Materials Engineering, Lund University, S-221 00 Lund, Sweden. Contact e-mail: martin.friis@htu.se.

particle properties. These properties must be representative of the process, must describe its state and fluctuations well, and moreover, be controllable.

Two such particle properties are the particle velocity (V) and the particle temperature (T), which both affect the subprocesses in the deposition process such as splat formation and solidification and interaction between the impacting droplet and underlying material.[1-6] Since V and T thereby also influence the final coating properties,[7] these two particle parameters are chosen as the relevant particle properties.

The particle velocity and particle temperature are, however, strongly positively correlated as an inherent feature of the plasma process.[8] This aggravates evaluation of their individual influence on the coating property unless proper measures are taken.

The way to control V and T individually by means of different spray gun parameters can be evaluated by a factorial designed experiment.[8] The objective of the experiment is twofold. First, it should point at one spray gun parameter having the largest effect on the magnitudes of V and T, and second, it should point at one spray gun parameter enabling separation of the velocity from the temperature. Thus, two relevant spray gun parameters must be determined.

By setting these two spray gun parameters to their maximum and minimum levels, in all four possible combinations, a subarea in the V-T plane can be found, within which it is possible to control V and T independently of each other.

Through the knowledge of how to independently control V and T, a design experiment based on V and T can be set from which final coating properties can be investigated. This enables evaluation and determination of the individual effect of V and T on different coating properties. By multiple linear regression, the mathematical models, and thus, process maps for each coating property of interest are created.

The mathematical models can then be used to plot contour levels of coating properties in V-T diagrams, with each diagram explaining the individual influence of V and T on a specific coating property. Each such contour plot constitutes a process map, and it should be noticed that the models are valid only within the sub-area in the V-T plane.

Specification of the allowed variation for each final coating property results in a band in the process map. By superimposing such bands, one for each relevant final coating property, a process window[9] is defined as the common area of all bands. By monitoring and controlling V and T to be within the process window through proper adjustments of the chosen spray gun parameters, the resulting coating will fill the request with respect to the required final coating properties.

If, however, it turns out that no such area common to all bands exists, this would mean that a coating with such a specification is impossible to produce.

3. Experimental

3.1 Material and Equipment

In the current study, thermal barrier coatings were deposited at a standoff distance of 70 mm by air plasma spray onto button-shaped Hastelloy samples, 6 mm thick and 25 mm in diameter. The material used for the bond coat was a NiCoCrAlY powder, and the topcoat powder was an yttria-stabilized zirconia powder (−90 + 19 μm), Amperit (H.C. Starck, Goslar, Germany). In total, 13 experiments including 4 used for verification were performed. In all treatments, zirconia powder from the same lot containing similar size distribution was used to deposit top coatings of 390-470 μm thickness.

The coatings were produced using a SM-F-100 Connex gun (Sulzer Metco, Wholen, Switzerland), controlled by an automated and robotized Sulzer Metco A3000 air plasma unit. The samples were mounted on a cylindrical fixture with a diameter of 133 mm that rotated during coating deposition. Particle velocity and particle temperature were measured prior to each coating deposition using the optical system DPV 2000 (Tecnar Automation Ltd, St-Hubert, Quebec, Canada). See Ref. 8 concerning the technique of using the DPV 2000 and the correctness of the measurements.

3.2 Microstructure Evaluation

The samples were vacuum impregnated with epoxy and cured, cut with a precision diamond wheel cut-off machine, and then impregnated again. Grinding and polishing were performed using an automatic polishing machine following a strict procedure. A careful plane grinding of 0.7 mm on stone was followed by a coarse polishing using a 9 μm, 6 μm, and 3 μm diamond suspension. Final polishing was performed using an oxide polishing suspension with approximately 0.04 μm grain size. Control of the preparation procedure was performed, and the preparation was found satisfactory when no trace of smearing, pullout effects, or penetration failure of the epoxy were found.

Evaluation of the coating microstructure was performed by image analysis on images acquired by scanning electron microscope (SEM). To prevent influence of the image quality on the image analysis result, a strict procedure for image acquisition by SEM was adapted and used. The SEM QBSD (four-quadrant back-scattered detector) was used in composition mode, and parameters such as acceleration voltage, working distance; brightness, and contrast were set to constant values. Thereafter, the beam current was used to adjust the image so that the highest peak, representing the coating material, in the gray scale histogram of the image pixels was situated at gray scale level 128. In this way all images were made to have similar gray scale representation. Figure 1 shows how the cumulative sum of total porosity evens out at approximately 10-15 images, after which no large deviations from the achieved mean value occurs. A total of 20 images at the resolution 768 × 768 pixels, where 768 pixels correspond to 135 μm and equal a magnification of 2120×, were acquired for each sample. These 20 images represent the whole cross section of the coating and achieve a steady representative mean value of each microstructure feature.

Transformation of the gray scale (0-255 gray scales) image into a binary (black-white) image was performed using two filters of different size to compare each pixel of the gray scale image, positioned in the middle of the filter, with the mean value of the pixels covered by the filter. The middle pixel was assigned to be black if darker, and white if brighter, than the mean gray scale value of the surrounding pixels. The smaller filter is sensitive to small variations in small parts of the image and creates an image with all details, but a lot of noise is also present. The larger filter is less sensitive to small variations and therefore prevents noise, resulting in a less detailed but noiseless image. With the assumption that at least a bit of a trace of all defects are

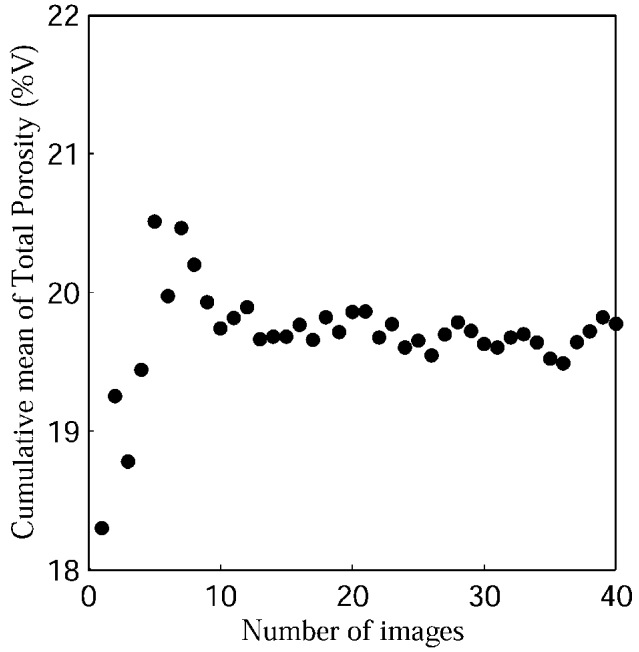

Fig. 1 Evolution of the cumulative mean value of total porosity concerning Sample 9

present in the image created by the large filter, the two images can be merged into a final binary image containing all details of the defects and no noise. This method, in contrast to thresholding, is operator independent.

The image analysis routine separates pores from cracks, based on aspect criterion, and saves respective features in two separate images. Analysis of the pore image results in the number of pixels present in each individual pore, while the crack image is analyzed more thoroughly. First, the total number of pixels present in cracks is analyzed, and then the cracks are shrunk to a skeleton of one pixel width and separated at each intersection. Thereafter, each crack is analyzed individually, resulting in the determination of the amount of pixels present and the angle of the crack.

The correctness of the microstructure evaluation was investigated by comparing results computed from three individually different image analysis routines. The results all showed similar trends with negligible deviation, and comparison with measurements performed using the water immersion technique showed a systematical mean deviation of 2% units. The method presented in this work is, in itself, general and not dependent on the accuracy of the measurements. It is, however, of vital importance that the degree of accuracy is consistent between measurements.

The microstructure was classified into four different types of features: namely, small pores defined to have a diameter less than 15 μm, large pores with a diameter above 15 μm, cracks, and total porosity, which include all defects. The partition limit, to separate small pores formed in and between splats from larger pores covering multiple splat thickness in height and width, was chosen to correspond to the thickness of a few splats.

3.3 Statistical Analysis

The influence of the particle velocity and particle temperature on the different microstructure features, i.e., total porosity, small pores, and large pores, and on the deposition efficiency, was analyzed by means of multiple linear regression. For each relation the assumed model was:

$$X_m = \beta_0 + \beta_V \cdot (V - \overline{V}) + \beta_T \cdot (T - \overline{T}) + \beta_{VT} \cdot (V - \overline{V}) \cdot (T - \overline{T}) + \beta_{V^2} \cdot (V - \overline{V})^2 + \beta_{T^2} \cdot (T - \overline{T})^2 \quad \text{(Eq 1)}$$

where X_m denotes either the microstructure feature or the deposition efficiency, V the particle velocity, $\overline{V}$ the arithmetic mean value of the velocity, T the particle temperature, and $\overline{T}$ the arithmetic mean value of the temperature. Furthermore, β_i denotes the regression coefficients for the different parameters indexed i accordingly.

The significance of the coefficients in the models were evaluated using the backward elimination method.[10] This method utilizes hypothesis testing, a partial F-test at a 95% confidence level, with only significant parameters included in the final models. The coefficients of determination, R^2, describing the percentage of the response variation the equations can account for, were also calculated.

3.4 Control of the Particle Properties and Experimental Design

In this work the spray gun current (C) and primary gas flow, argon (A), were chosen to control the particle velocity and particle temperature, since these have been shown to be the most important parameters controlling the particle properties,[4,8] for the present spray gun. The spray gun current controls the power input into the plasma; high power input results in both high velocity and high temperature of the particles. Argon flow rate is the only spray gun parameter having an inverse influence on the particle velocity and particle temperature and is used to separate the two properties. Higher argon flow rates result in higher particle velocity and lower particle temperature, and vice versa.

The process sub-areas in the V-T plane were found by varying C and A between their extreme values, 250-450 A and 25-50 standard liters per minute (slpm), respectively, in all four possible combinations, and by measuring the corresponding particle velocity and particle temperature. This resulted in the four points, I-IV, constituting the boundaries of the area within which V and T are controllable (Fig. 2).

All other spray gun parameters were kept at constant levels during spraying of the different experimental treatments (Table 1). In addition, the voltage did not vary significantly. A large number of particles were observed by DPV 2000 for each particle measurement operation.

An experimental design was determined to fulfill two main ideas, namely, to cover the process sub-area, and to vary V and T independently of each other. Accordingly, the experimental set points were chosen as shown in Fig. 2 (squares), with a velocity interval of 20 m/s and a temperature interval of 90° between the points.

To achieve the set points in Fig. 2, the following procedure was applied. First, the design values of V and T for a specific point of interest were used to calculate the initial values of C and A from Eq 2 and 3. Second, V and T were measured, with these initial values of C and A setting the spray gun. Third, the setting

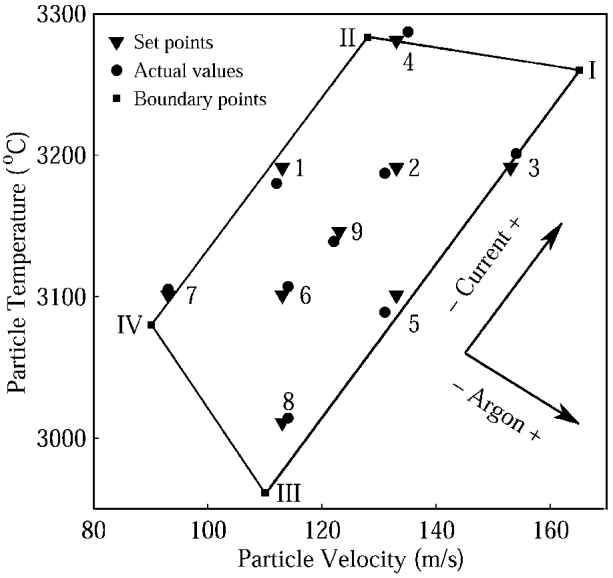

Fig. 2 The sub-area in the *V-T* plane with corresponding boundary points I-IV together with the experimental set points and actual values 1-9. The triangles represent the experimental set points and the circles represent the actual values. The black arrows indicate the influence of current and argon, respectively, on the particle velocity and temperature.

Table 1 Process Parameter Settings

Parameter	Setting
Secondary gas flow	4 slpm H_2
Carrier gas flow	2 slpm H_2
Powder feed rate	40 g/min
Turn table rotation speed	75 rpm
Spray gun vertical velocity	5 mm/s
Spray distance	70 mm
Spray angle	90°
Substrate temperature	100 °C

of *C* and *A* were adjusted based on experience, and *V* and *T* were measured again, until a close enough fit was achieved. The trend of the influence of current and argon on the particle velocity and particle temperature is included in Fig. 2.

An average of three settings and corresponding measurements of *V* and *T* were necessary to find each experimental design point. The coefficients of Eq 2 and 3 were updated for each new measured point.

The experiments resulted in the following dependence of *V* and *T* on *C* and *A* through multiple linear regression models:

$$\textit{Particle Velocity}\ (m/s) = 123.0 + 0.2379 \cdot (C - \overline{C}) + 1.0484 \cdot (A - \overline{A}) + 0.0029 \cdot (C - \overline{C}) \cdot (A - \overline{A})\ R^2 = 0.976 \quad \text{(Eq 2)}$$

$$\textit{Particle Temperature}\ (°C) = 3161 + 1.19 \cdot (C - \overline{C}) - 3.15 \cdot (A - \overline{A}) + 0.016 \cdot (C - \overline{C}) \cdot (A - \overline{A}) - 0.14 \cdot (A - \overline{A})^2\ R^2 = 0.955 \quad \text{(Eq 3)}$$

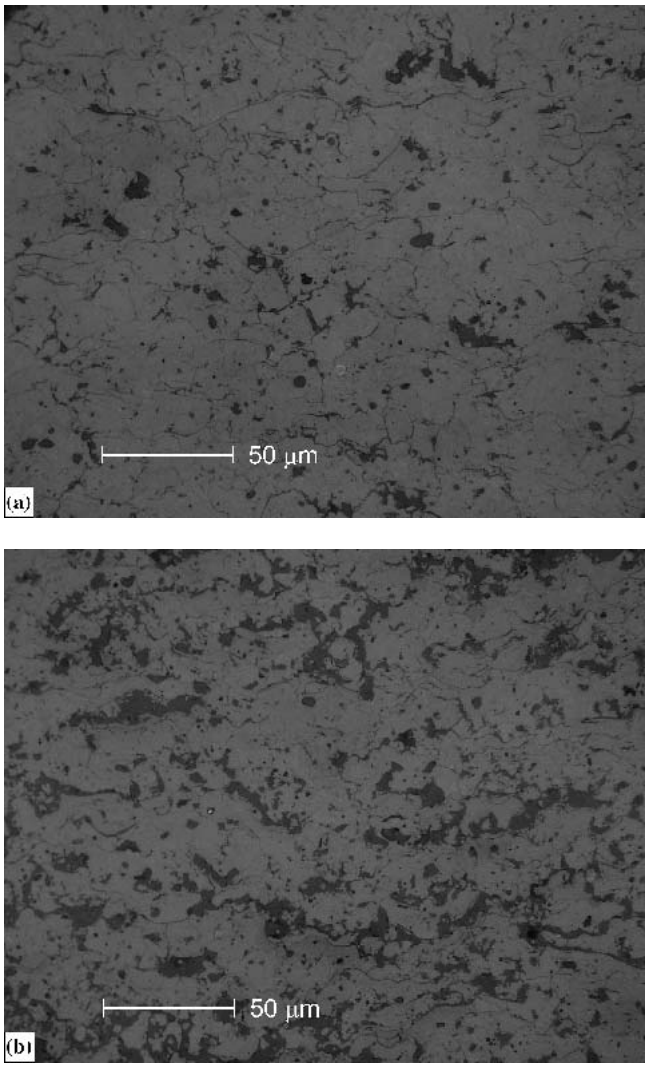

Fig. 3 **(a)** Image of the dense microstructure present in Sample 4; **(b)** image of Sample 8 showing porous microstructure

The relations assume that *C* is measured in amperes and *A* in standard liters per minute. The coefficients of determination, R^2, for Eq 2 and 3 are above 0.95, which means that the spray gun parameters *C* and *A* very well control the particle velocity and particle temperature. This is also obvious from the small deviation between the experimental set points and actual values (Fig. 2).

4. Experimental Results

4.1 Process Maps

Total porosity is defined here as the sum of all existent features of the microstructure, i.e., small pores, large pores, and cracks. The amount of total porosity in the nine samples examined in the current study could be varied from 16-24% by controlling the particle velocity from 93-153 m/s and the particle temperature from 3011-3281 °C.

The difference in total porosity is visualized in Fig. 3 (a and b), where images of the dense sample resulting from point #4 in

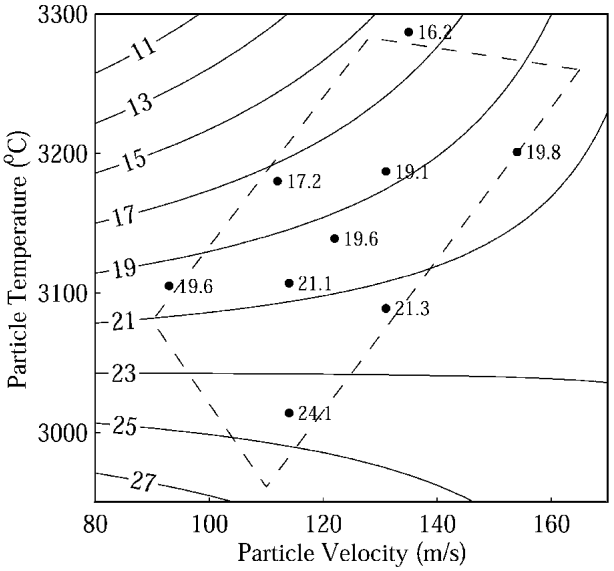

Fig. 4 Process map showing the influence of particle velocity and temperature on the volume percentage of total porosity together with the total porosity values for each experimental point

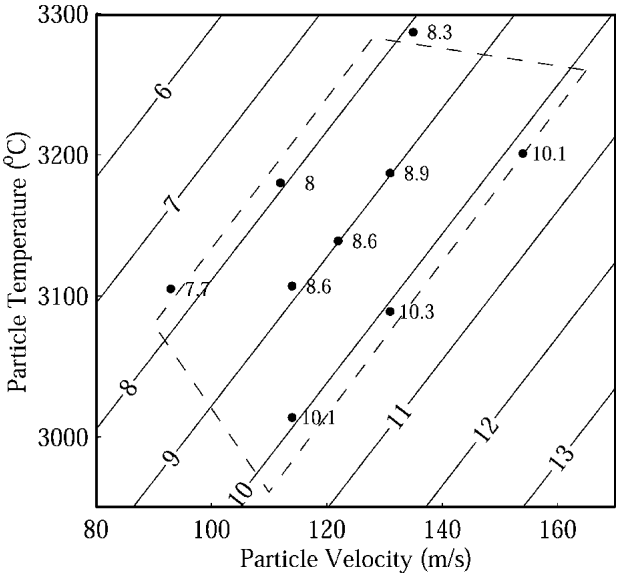

Fig. 5 Process map of small pores together with the amount of small pores for each experimental point

Fig. 2 and the porous sample resulting from point #8 in Fig. 2 are shown. The influence of particle velocity and particle temperature on the total porosity was evaluated by multiple linear regression, and the resulting equation having a coefficient of determination $R^2 = 0.98$ is visualized in Fig. 4. It should be noticed that the equation is strictly valid within the sub-area marked in Fig. 4.

An increase in particle velocity results in an increase of total porosity, except in the lower temperature region, while an increase in particle temperature results in a decrease. Moreover, the interaction effect between the particle velocity and particle temperature on the total porosity is significant. This means that the impact on the total porosity of a specific change in one of the particle properties to a certain extent depends on the value of the other particle property. For example, changing the particle velocity 40 m/s will affect the total porosity differently at a constant high particle temperature as compared to a low constant particle temperature. The same reasoning is valid for the particle temperature (Fig. 4).

The amount of small pores varied from 8-10%. In Fig. 5 the regression equation describing the influence of particle velocity and temperature on small pores is visualized. The equation has a coefficient of determination $R^2 = 0.95$, which means that V and T very well describe the variation in the amount of small pores.

The amount of small pores increases with increasing particle velocity and decreasing particle temperature. Particle velocity affects the degree of particle splashing, meaning that a higher particle velocity causes the particle fringes to scatter, thereby creating opportunities for small cavities and crevices to form. The particle temperature affects the viscosity of the particles so that low particle temperatures imply high viscosity and, thus, a low ability of the droplet to fill the existing crevices and irregularities present at the underlying surface.

The feature of large pores varied from 2-8%. Only particle temperature proved to have a significant influence on large pores

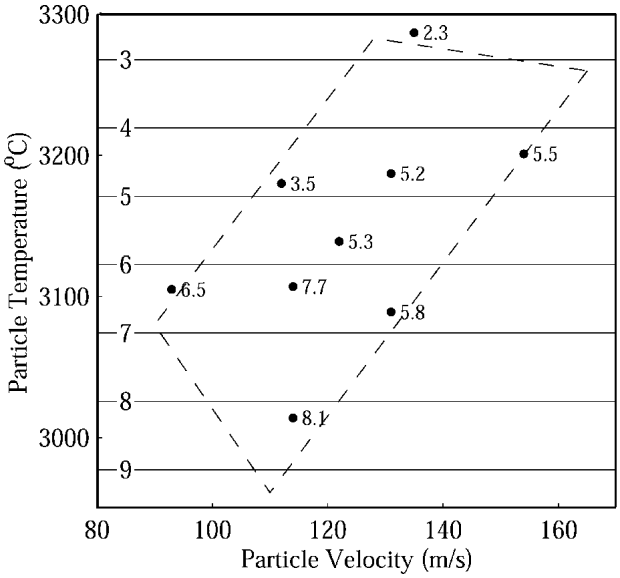

Fig. 6 Process map of large pores together with the amount of large pores for each experimental point

according to the regression evaluation ($R^2 = 0.77$). This relation is visualized in Fig. 6. The amount of large pores increases with a decrease of the particle temperature.

An important characteristic and an economical aspect of the plasma spray process is the deposition efficiency. The percentage of the deposition efficiency is explained by the influence of the particle properties through a regression equation, visualized in Fig. 7. Distinctive agreement in the variation of deposition efficiency and particle velocity and particle temperature was found, which is emphasized by the very high coefficient of determination, $R^2 = 0.98$. The deposition efficiency increases with

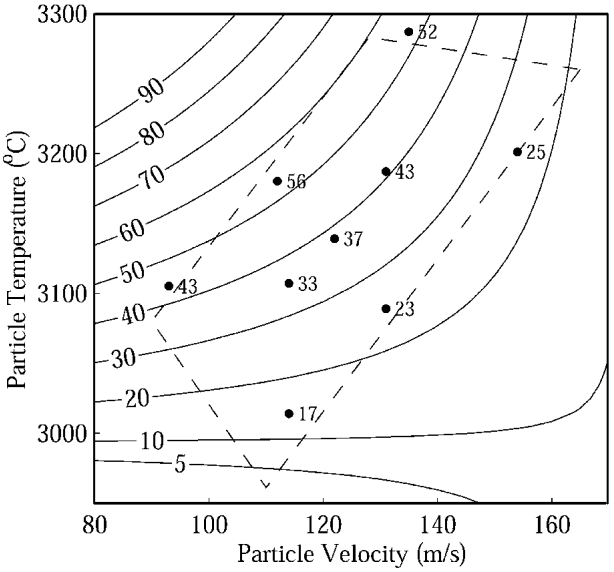

Fig. 7 Process map of deposition efficiency together with the deposition efficiency for each experimental point

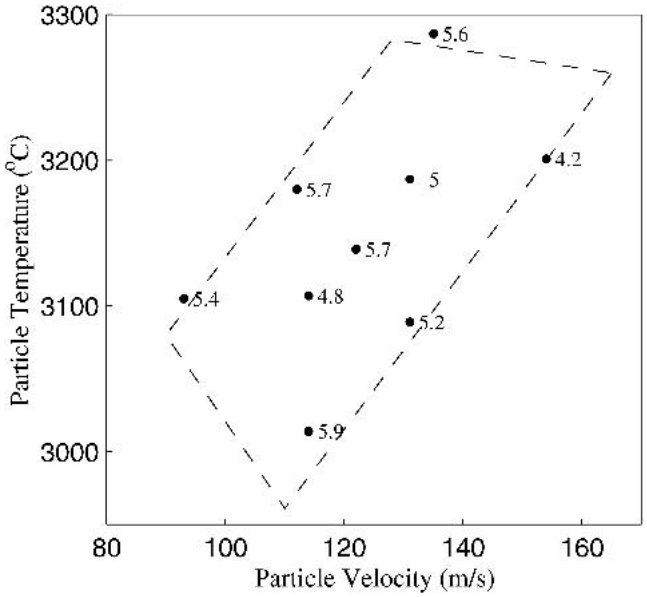

Fig. 8 Influence of particle velocity and temperature on the volume percentage of all cracks

decreasing particle velocity and with increasing particle temperature. Moreover, the interaction between V and T has a significant influence, as seen in Fig. 7, through the large nonlinearity of the contour lines.

4.2 Cracks

The total amount of cracks varied from 5.9-4.2 vol.%, i.e., at most 1.7% units, between the nine samples, but no obvious pattern of the difference in crack volume percentage was found (Fig. 8).

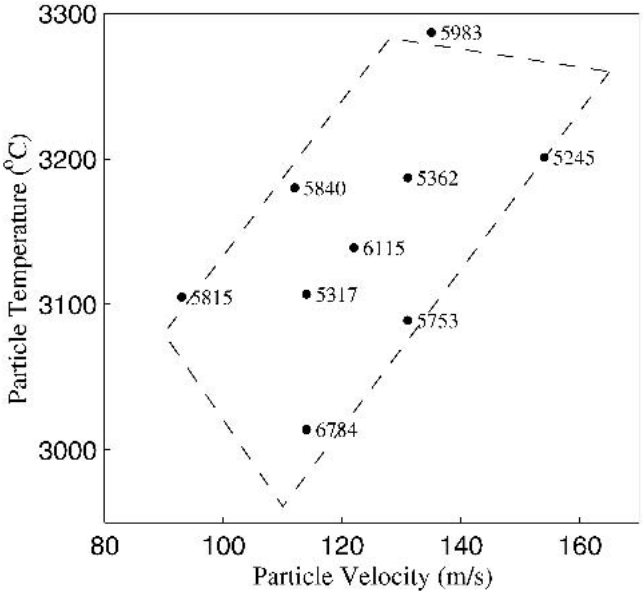

Fig. 9 Influence of particle velocity and temperature on the amount of pixels present in the skeletonized cracks having an angle of 0 ± 45°

In pursuing the analysis, the cracks were classified into two different types: namely, delaminations, i.e., cracks parallel with the substrate surface ±45°, and vertical cracks, i.e., cracks perpendicular to the substrate surface ±45°. The total amount of pixels present in each sample relating to delaminations is shown in Fig. 9, while the amount of vertical cracks is shown in Fig. 10. The distribution pattern of the amount of delamination pixels was similar to the one for total amount of cracks. The largest amount of vertical cracks was found in the sample numbers 1, 4, 9, 2, and 7. A comparison with the process map of deposition efficiency (Fig. 7) reveals that these samples were sprayed with high deposition efficiency, implying creation of vertical cracks to be enhanced at coating deposition with large passage thickness, which is a direct consequence of the high deposition efficiency. However, the regression analysis showed that neither particle velocity nor particle temperature had a significant influence on the total amount of cracks, neither on delaminations nor vertical cracks. Process maps could therefore not be created.

The crack angle distribution was studied and showed no large variation between the samples. This contradicts findings by Prystay et al.,[4] who showed that a significant change in the crack angle distribution could be achieved by increasing the particle temperature 164 °C, while keeping the particle velocity constant. In Fig. 11 the crack angle distribution for Samples 4 and 5, deposited with a particle temperature difference of 197 °C at constant particle velocity, is shown, and no significant difference is found. Furthermore, only a small difference is detected when comparing the samples having the largest and the smallest volume percentage of cracks (Fig. 12). The possible origin of the discrepancy between these two investigations may be that in Prystay et al.[4] both pores and cracks are skeletonized to 1 pixel width by the image analysis. Consequently, pores are included in the crack angle distribution analysis. In the present work all pores are separated from the image, with the result that only features characterized as cracks are skeletonized and included in the crack angle distribution analysis. As has been shown, the

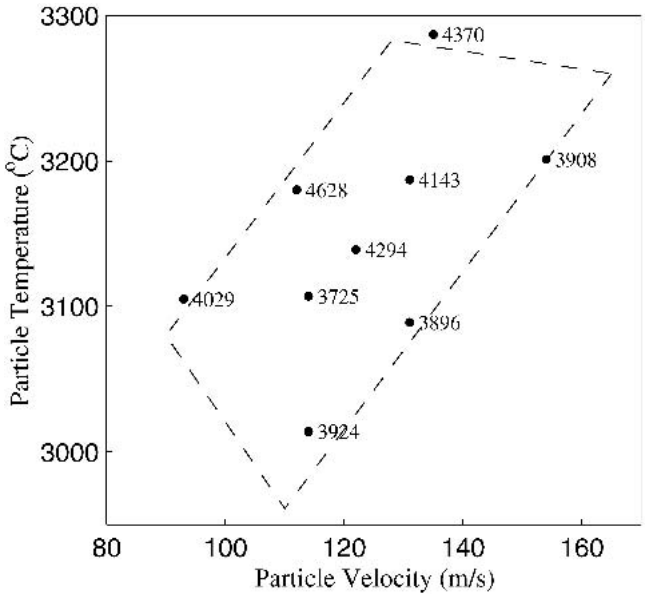

Fig. 10 Influence of particle velocity and temperature on the amount of pixels present in the skeletonized cracks having an angle of 90 ± 45°

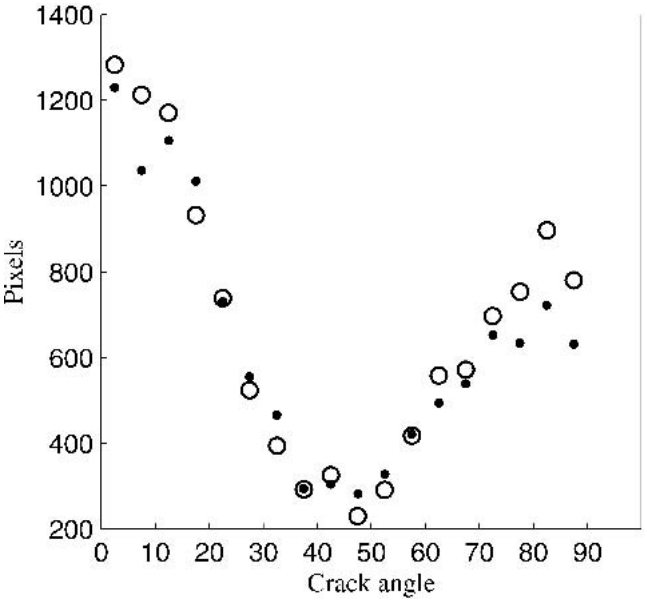

Fig. 11 Crack angle distribution for two coatings deposited at a particle temperature of 133 m/s and a particle temperature of 3287 °C concerning Sample 4 (○) and 3090 °C concerning Sample 5 (•)

amount of pores is highly dependent on particle velocity and particle temperature and therefore, varies accordingly.

4.3 Controlling the Process by a Process Window

In a previous work, a method to create a process window with the aim to perform on-line control of the particle properties was presented.[9] This method defines the boundaries within which the particle properties have to be kept to ensure the requirements concerning the microstructure features of the coating to be fulfilled. For this method to be successful, the residuals of the models describing each microstructure feature have to be significantly smaller than the size of the tolerance range.

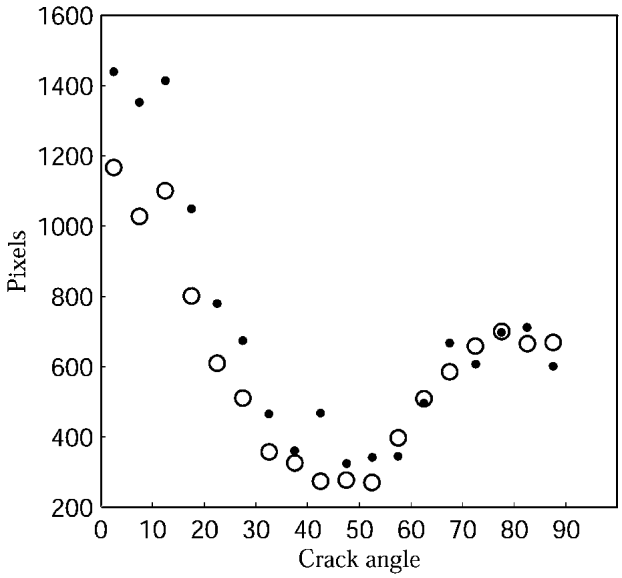

Fig. 12 Crack angle distribution for Sample 8 (○) deposited at a particle temperature of 114 m/s and a particle temperature of 3014 °C, and Sample 3 (•) deposited at a particle temperature of 154 m/s and a particle temperature of 3201 °C

Verification of the process window method relying on the process maps was performed by specification and creation of process windows (Fig. 13), and deposition of two different coatings, one porous and one dense, according to the specifications given in Fig. 14, at a substrate temperature (T_S) of 100 °C.

Additionally, an attempt was made to produce identical coatings at a substrate temperature of 400 °C. To achieve this, the effect of the substrate temperature difference on the different microstructure features[7] was added to the regression equations, and new process maps and additional process windows were created (Fig. 13). This implies that the effect of the substrate temperature on the microstructure features had to be compensated for by changing the particle velocity and temperature (Fig. 13).

The particle velocity and particle temperature, for each coating deposition, were aimed at the geometrical center point of the corresponding process window (Fig. 13), which also presents the attained values. As shown by the figure, the correspondence is satisfactory.

The specifications concerning total porosity, small pores, and deposition efficiency were fulfilled, while the amount of large pores was slightly higher than the specifications (Fig. 14). This might be because large pores are not as well explained by V and T as the other features, i.e., the size of the tolerance range is small compared with the residuals.

5. Discussion

It has been found that the coating microstructure, e.g., amount of porosity, is well explained by particle velocity and particle temperature. This enables on-line particle diagnostics as a powerful tool to control the process. Better process knowledge and process control provide the means to produce a coating with

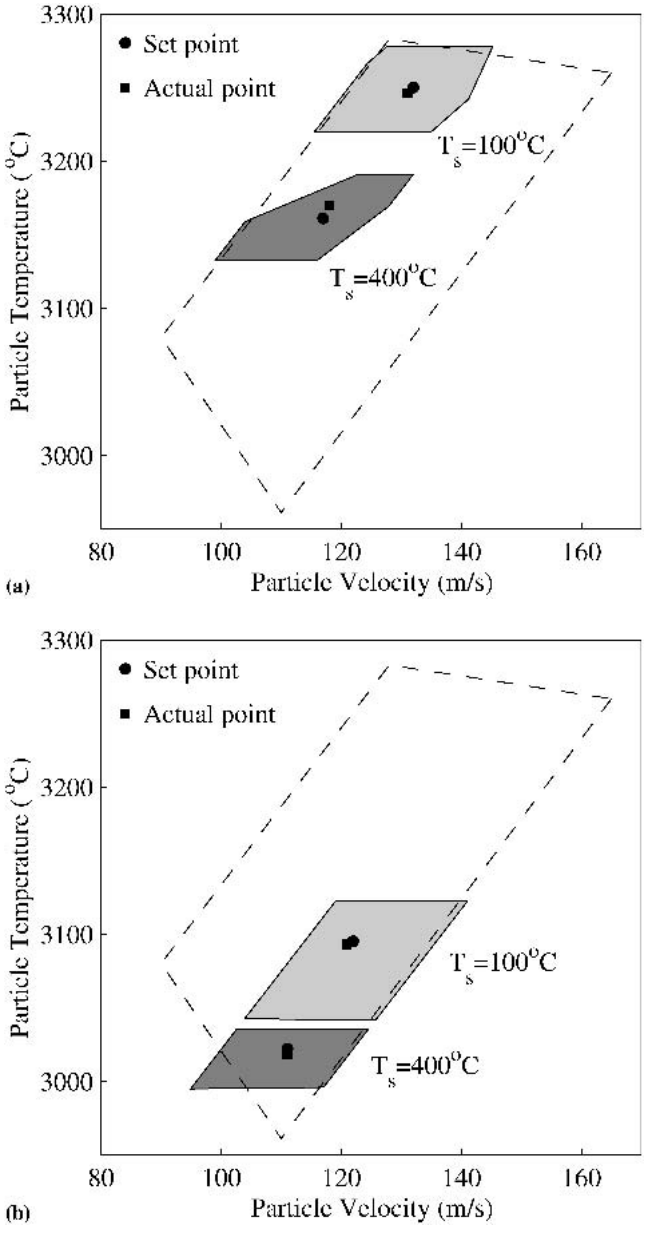

Fig. 13 **(a)** Two process windows for a compact coating produced at a substrate temperature of 100 and 400 °C; **(b)** two process windows for a porous coating produced at a substrate temperature of 100 and 400 °C

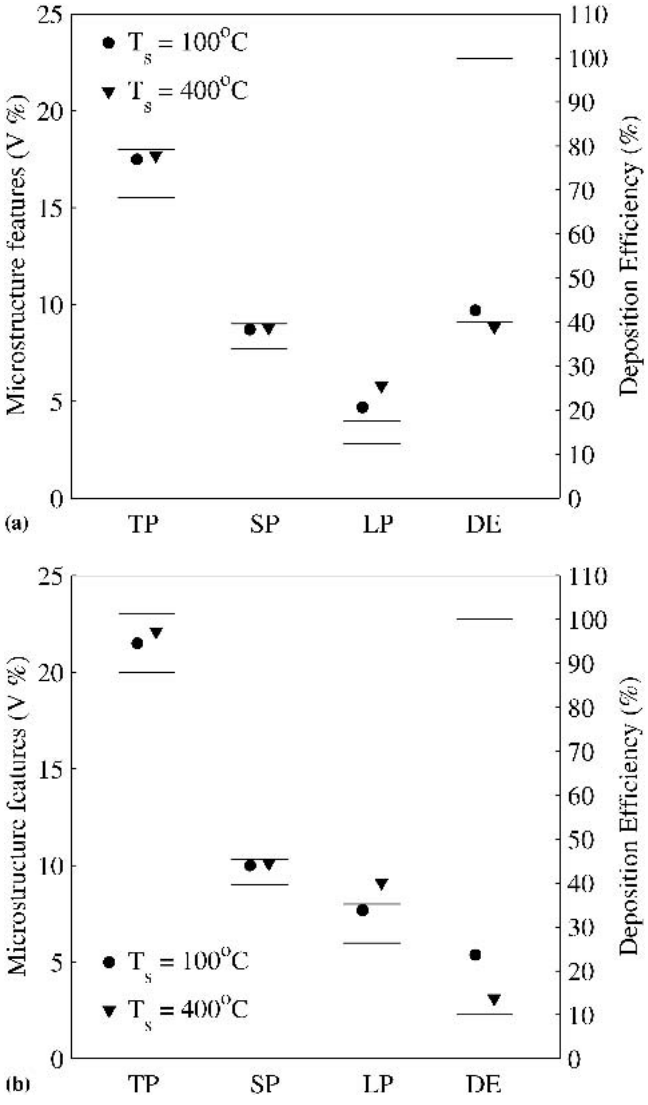

Fig. 14 **(a)** The diagram presents the specification limits as solid lines together with the resulting values of the two compact coatings. **(b)** The diagram presents the specification limits as solid lines together with the resulting values of the two porous coatings. TP, Total Porosity; SP, Small Pores; LP, Large Pores; and DE, Deposition Efficiency.

a specific microstructure, and thereby optimize the performance of the coating.

A straightforward approach to systematize process knowledge is to create process maps describing the individual effect of *V* and *T*, respectively, on the coating microstructure. Process maps can also be constructed for other responses, e.g., deposition efficiency. When process maps are available for the coating properties of concern, it is possible to construct a process window from the coating specification, providing the process limits for *V* and *T*.

However, *V* and *T* are strongly correlated. It has been shown that it is possible to separate them using the spray gun current and the primary gas flow,[4,7] in this case argon. In this work this knowledge has been used to stretch out and cover a large area in the *V*-*T* plane, which makes it possible to use each spray gun in its full range and to produce coatings with widely different microstructures.

A result worth noticing is that a similar amount of total porosity can be achieved with totally different settings of the particle velocity and particle temperature. For example, points #3, #7, and #9 vary in particle velocity with an interval of 30 m/s and particle temperature in intervals of 45 °C between each point and stretch over the whole sub-area in the *V*-*T* plane (Fig. 2). These settings result in almost the same total porosity, namely 19.6%, 19.6%, and 19.8%. The explanation is obvious when comparing the three points in Fig. 2 with corresponding positions of *V* and *T* in Fig. 4. They all fall on the same contour line of total porosity. When following the contour line it is clear that the effect of increasing *V* is compensated by the effect of increasing *T*.

However, the constitution of this microstructure, although having the same total porosity, is bound to differ, which is obvious when comparing the other features' values at these three points. Assuming the different features to have different impact on, for example, thermal conductivity, it can be concluded that it is now possible to produce coatings with equal total porosity having different thermal conductivity. The knowledge of how to control the individual features of the microstructures enables tailor-made coatings to be produced.

Although the models well describe each individual feature of the microstructure, shown by the very high values of the coefficient of determination R^2, it is not possible to create a coating with an arbitrary constitution. This is because a specific particle property has different influence on different features, e.g., a high particle velocity increases the amount of total porosity but it decreases the deposition efficiency, i.e., the features are correlated.

A specifically important high correlation is the one between total porosity and deposition efficiency. This correlation is very high, and negative, which implies that producing a very porous coating has to be done with settings of the particle velocity and particle temperature resulting in very low deposition efficiency, and vice versa.

Neither V nor T showed any significant influence on the amount of cracks. However, it has been shown that cracks are influenced by other parameters such as the substrate temperature.[7] The coatings deposited at substrate temperatures of 100 and 400 °C showed a difference of 1 vol.% unit in the amount of cracks, which agrees with results found in Ref. 7.

6. Conclusion

It has been shown that individual control of the particle velocity and particle temperature can be achieved satisfactorily by specifically selected spray gun parameters within limitations, specific for each spray gun and powder.

This knowledge enables a designed experiment based on the particle velocity and temperature to be performed, resulting in process maps explaining the individual effect of V and T on each coating property of concern.

The method of process windows,[9] employing the process maps, enables a desired coating microstructure to be specified and manufactured. Monitoring and controlling particle velocity and particle temperature to keep within the process window ensure the desired coating microstructure.

Acknowledgment

The authors gratefully acknowledge fruitful discussions and writing inspiration from Dr. Solveig Melin. The authors gratefully acknowledge valuable discussions with Mr. Jan Wigren, Dr. Lars Pejryd, and Dr. Per Nylen, and the Volvo Aero Corporation, Trollhattan, Sweden, for enabling the experiments required for this work. The authors acknowledge the financial support from the Foundation for Knowledge and Competence Development and EC Structural Founds.

References

1. M. Vardelle, A. Vardelle, P. Fauchais, and C. Moreau: "Pyrometer System for Monitoring the Particle Impact on a Substrate During a Plasma Spray Process," *Meas. Sci. Technol.*, 1994, *5*, pp. 205-12.
2. P. Fauchais, M. Vardelle, A. Vardelle, and L. Bianchi: "Plasma Spray: Study of the Coating Generation," *Ceramic Int.*, 1996, *22*, pp. 295-303.
3. M. Vardelle, A. Vardelle, A.C. Leger, P. Fauchais, and D. Gobin: "Influence of Particle Parameters at Impact on Splat Formation and Solidification in Plasma Spraying Processes," *J. Therm. Spray Technol*, 1995, *4*(1), pp. 50-58.
4. M. Prystay, P. Gougeon, and C. Moreau: "Structure of Plasma-Sprayed Zirconia Coatings Tailored by Controlling the Temperature and Velocity of the Sprayed Particles." *J. Therm. Spray Technol.*, 2001, *10*(1), pp. 67-75.
5. M. Vardelle, A. Vardelle, A.C. Leger, and P. Fauchais: "Dynamics of Splat Formation and Solidification in Thermal Spraying Process" in *Thermal Spray Industrial Applications*, C.C. Berndt and S. Sampath, ed. ASM International, Materials Park, OH, 1994, pp. 555-62.
6. A.C. Leger, M. Vardelle, A. Vardelle, P. Fauchais, S. Sampath, C.C. Berndt, and H. Herman: "Plasma Sprayed Zirconia: Relationships Between Particle Parameters, Splat Formation and Deposit Generation—Part I: Impact and Solidification" in *Thermal Spray: Practical Solutions for Engineering Problems*, C.C. Berndt, ed., ASM International, Materials Park, OH, 1996, pp. 623-28.
7. M. Friis, C. Persson, and J. Wigren: "Influence of Particle In-Flight Characteristics on the Microstructure of Atmospheric Plasma Sprayed Yttria Stabilized ZrO2," *Surf. Coat. Technol.*, 2001, *141*(2-3), pp. 115-27.
8. M. Friis, P. Nylen, C. Persson, and J. Wigren: "Investigation of Particle In-Flight Characteristics During Atmospheric Plasma Spraying of Yttria Stabilized ZrO2: Part 1. Experimental," *J. Therm. Spray Technol.,* 2001, *10*(2), pp. 301-10.
9. M.Friis and C.Persson: "Process Window for Plasma Spray Processes," in *Thermal Spray 2001: New Surfaces for a New Millennium*, C.C. Berndt, K.A. Khor, and E. Lugscheider, ed., ASM International, Materials Park, OH, 2001, pp. 1313-19.
10. N.R. Draper and H. Smith: *Applied Regression Analysis,* 3rd ed., John Wiley & Sons Inc., NY, 1995.